ACS central science

Research Article

http://pubs.acs.org/journal/acscii

Combinatorial Discovery of Defined Substrates That Promote a Stem Cell State in Malignant Melanoma

Douglas Zhang,[†] Junmin Lee,[†] Michael B. Sun,[†] Yi Pei,[†] James Chu,[‡] Martha U. Gillette,[‡] Timothy M. Fan,[§] and Kristopher A. Kilian*[,†,∥]

[†]Department of Materials Science and Engineering, [‡]Department of Cell and Developmental Biology, [§]Department of Veterinary Clinical Medicine, and [∥]Department of Bioengineering, University of Illinois at Urbana−Champaign, Urbana, Illinois 61801, United States

Supporting Information

ABSTRACT: The tumor microenvironment is implicated in orchestrating cancer cell transformation and metastasis. However, specific cell−ligand interactions between cancer cells and the extracellular matrix are difficult to decipher due to a dynamic and multivariate presentation of many signaling molecules. Here we report a versatile peptide microarray platform that is capable of screening for cancer cell phenotypic changes in response to ligand−receptor interactions. Using a screen of 78 peptide combinations derived from proteins present in the melanoma microenvironment, we identify a proteoglycan binding and bone morphogenic protein 7 (BMP7) derived sequence that selectively promotes the expression of several putative melanoma initiating cell markers. We characterize signaling associated with each of these peptides in the activation of melanoma pro-tumorigenic signaling and reveal a role for proteoglycan mediated adhesion and signaling through Smad 2/3. A defined substratum that controls the state of malignant melanoma may prove useful in spatially normalizing a heterogeneous population of tumor cells for discovery of therapeutics that target a specific state and for identifying new drug targets and reagents for intervention.

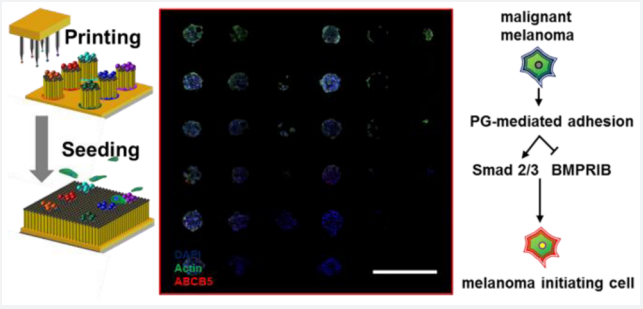

1. INTRODUCTION

Cutaneous melanoma is the most deadly form of skin cancer, with poor prognosis in patients with distant or recurring metastases.[1] Recent exploration into the pathogenesis of melanoma metastasis has revealed that a small subpopulation of melanoma-initiating cells (MICs), postulated to have characteristics of stem cells, correspond to increased metastatic progression.[2] Like traditional stem cells, these MICs are thought to be highly proliferative, self-renew, and have the capabilities of reconstituting all cells contained within the heterogeneous tumor environment.[3] The cancer stem cell hypothesis helps explain the perplexing and poorly understood clinical phenomena where a patient with cancer may have robust response to chemotherapy treatment only to have eventual relapse.[4] As such, studies aimed at classifying MICs could provide new insights into disease progression and assist in the identification of this dangerous subpopulation of cells for therapeutic targeting.

Several recent high profile studies have presented evidence that MICs are much more common than previously appreciated, and that no single surface marker can distinguish between a tumorigenic and non-tumorigenic phenotype.[5,6] Although these disparate results seem to challenge the classical cancer stem cell model in which only a subset of cells are capable of tumor formation, this model is not mutually exclusive with a more traditional stochastic model that postulates that all tumor cells are capable of tumor formation and progression.[7] Furthermore, factors such as environmental cues can facilitate a phenotypic change between cancer and noncancer stem-like cells.[8,9] In fact, increasing efforts to elucidate the role of the microenvironment on the progression of cancer has identified elements of the tumor microenvironment as important prognostic and predictive indicators of metastasis.[10,11] These elements include perivascular cells and the cytokine and growth factor network they secrete,[12] integrins,[13] the extracellular matrix protein composition[14] and surrounding stroma,[15] as well as the mechanical properties of the stroma.[10] Taken together, these studies suggest that when thinking about MICs, we should also consider the biophysical and biochemical characteristics of the tumor microenvironment in which they reside.

To explore how microenvironmental parameters can influence stem cell characteristics, high throughput approaches have been developed to screen for materials whose properties guide cell state and fate determination. Typically, high-throughput approaches to model the microenvironment have largely focused on characterizing cell response to the adhesive

Received: November 4, 2016
Published: April 26, 2017

DOI: 10.1021/acscentsci.6b00329
ACS Cent. Sci. 2017, 3, 381−393

properties of the substrates. Early work by Langer et al. exploited the use of robotic fluid handling to create arrays of polyacrylate monomers to study the effect of polymer-stem cell interactions.[16] Lutolf et al. used a DNA spotter to create cell niche microarray spots with modular stiffness (1−50 kPa) per well, along with various combinations of proteins to study proliferation, quiescence, and death of neural stem cells.[17] Kiessling and co-workers applied self-assembled monolayers (SAMs) on gold into an array type format investigating the effects of various peptide ligands on stem cell culture[18] and embryonal carcinoma cell binding capabilities.[19]

Recently these high-throughput screening techniques have enhanced our understanding of cancer cell adhesion-mediated signaling,[20] specifically the role of the extracellular matrix (ECM). Bhatia et al. used an array of ECM proteins to screen the adhesion profiles of primary and metastatic tumor cells and found that metastatic cells selectively associate with certain combinations of ECM molecules.[21] Peyton et al. combined ECM proteins to mimic the in vivo characteristics of bone, brain, and lung, and created a cellular phenotypic fingerprint of bone, brain, and lung metastasis that could predict metastatic tropism of other heterogeneous cell lines.[22] Furthermore, work by Hendrix et al. using ECM matrices secreted by human embryonic stem cells demonstrated that exposure of melanoma cells to the stem cell generated microenvironment was sufficient to reprogram the melanoma cells to a less malignant state.[23] These studies suggest that the biophysical and biochemical interactions between cancer cells and the matrix are key mediators of reprogramming and phenotype switching.[24] We hypothesize that a select combination of small peptides derived from proteins present in the ECM—that promote sustained interactions with specific surface receptors—will modulate intracellular signals to regulate the phenotype of melanoma cells in culture. Identification of defined surfaces that prime a specific cellular outcome holds great potential in applications such as drug screening, where a substrate can be tailored to augment a desired cancer cell state. Furthermore, identifying precise matrix signals that activate the elusive and deadly MIC state will reveal new pathways to guide therapeutic intervention.

In this paper we use a single-step peptide microarray chemistry[25] to explore the combinatorial presentation of short peptides that engage different classes of cell surface receptors displayed by adherent melanoma cells. We demonstrate that this array approach is able to identify unique peptide combinations that promote expression of MIC markers. Concurrent interaction with an adhesion and growth factor derived sequence reveals a role for each peptide in modulating the melanoma cell state, and identifies Smad 2/3 as a key signaling pathway in which these markers are upregulated. Functional studies suggest these cells adopt a stem-like phenotype; however, this phenotype is transient, and the cells will revert when returned to standard cell culture conditions, underscoring the potential to manipulate the plasticity of malignant melanoma. This approach provides a tool for exploring how cancer cells integrate multiple matrix signals to regulate metastatic potential and may prove useful as a platform for the development of drugs that target metastatic and tumorigenic cell populations.

2. RESULTS AND DISCUSSION

Biomimetic Peptides and Array Fabrication. Peptide microarrays have attracted significant attention as a screening tool, since short peptides can be presented uniformly on a substrate with an inert background, to unequivocally discern specific receptor−ligand binding interactions.[18,26] One caveat associated with using short peptides, particularly those derived from cytokines and growth factors, is the monomeric nature of the binding interface which could preclude important multimeric binding-downstream activity relationships. Growth factor derived peptides at high density have been shown to accommodate receptor activation similar to full-length proteins, while when presented at low density they may inhibit growth factor signaling.[27−30] These studies underscore the importance of understanding the relationships associated with ligand presentation and receptor signaling, when working with surface presenting short peptides.

Since the extracellular microenvironment during melanoma progression is host to a large combination of molecules that support cell adhesion, proliferation, migration, and differentiation among other activities,[31,32] we surveyed the literature to identify short oligomeric peptides between 3 and 12 amino acids in length that were reported to have bioactive properties.[33−41] We focused our search on three groups: integrin binding, proteoglycan binding, and growth factor derived peptides. Integrins are one of the most studied groups of signaling molecules and are known to play a key role in cellular adhesion as well as regulating cytoskeletal organization and transmembrane signal transduction.[42] Proteoglycans, especially heparin, are able to bind to many different classes of proteins including growth factors, cytokines, metabolic enzymes, and other structural proteins,[31] which highlights the importance of proteoglycans in signal regulation. Integrins and proteoglycans often act synergistically with other growth factor receptors[43] to regulate cell function and behavior.[44] We selected a subset of 12 peptides which were derived from major extracellular matrix proteins and growth factors (Table 1). We chose to investigate these 12 peptides individually and pairwise with each other (78 total combinations).

Table 1. Peptides and Derived ECM Sources

#	sequence	source
1	GRGDS[33]	fibronectin, vitronectin
2	YIGSR[34]	laminin
3	IKVAV[35]	laminin
4	FYFDLR[36]	collagen IV
5	KRSR[37]	laminin
6	FHRRIKA[38]	bone sialoprotein
7	SHWSPWSS[39]	hThrombospondin
8	DWIVA[40]	BMP-2
9	KPSSAPTQLN[41]	BMP-7
10	YSDKSLPHP	JAGGED
11	HYQASVSPEPP	DELTA-1
12	IPKVELVPAG	ACTIVIN-1

To investigate cell-ligand interactions on these peptides, we expanded and optimized our array spotting platform[25] to print circular islands of peptide-conjugated alkanethiolates (Figure 1a) onto gold coated coverslips. Each island contains either a single or pairwise peptide combination. We used coverslips approximately 25 mm × 25 mm, each containing 6 replicates of the 78 peptide combinations, 3 negative controls, and 3 positive controls, arranged into subarrays, for a total of 504 spots per coverslip (Figure 1b). Each spot is spaced 500 μm apart, and each subarray is spaced 1000 μm apart to easily differentiate

DOI: 10.1021/acscentsci.6b00329
ACS Cent. Sci. 2017, 3, 381−393

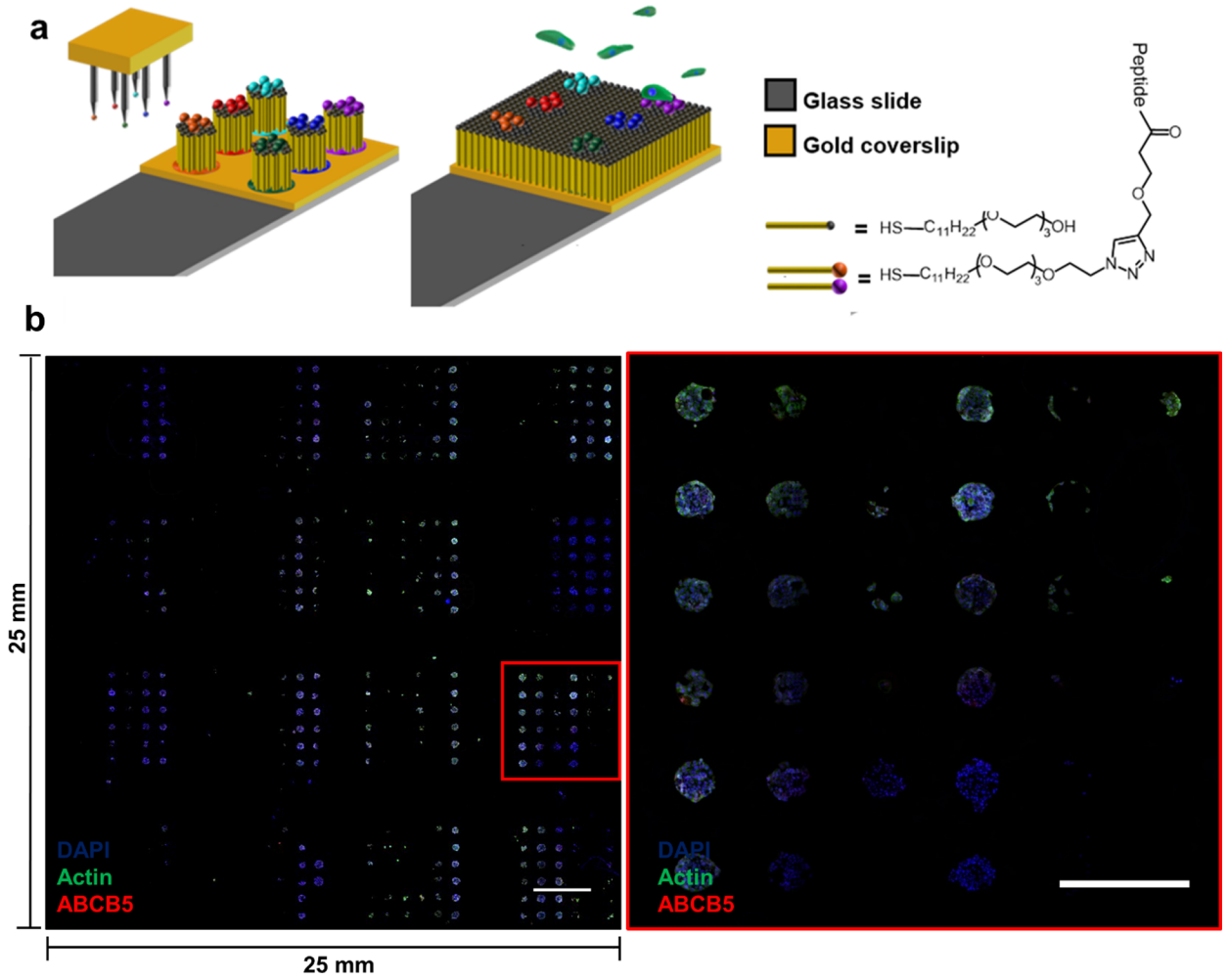

Figure 1. Schematic for generating peptide microarrays. An OmniGrid microarray spotter deposits nanoliters of a spotting solution containing EG3-terminating alkanethiols, and peptide-terminating alkanethiols onto a gold surface. A background EG3-terminating alkanethiol passivates the nonspotted regions, and seeded cells adhere only to peptide-terminated regions of the self-assembled monolayer (a). Representative image showing B16F0 melanoma cells adhering to the array (b) and a representative subarray (inset). Scale bar is 1500 and 700 μm for inset.

between subarrays. To fabricate the arrays, we created a master 384-well plate by pipetting peptide(s), a 15/85 mol/mol solution HS-C11-EG4-N3/HS-C11-EG3, and a click solution containing Cu(I), TBTA, and sodium ascorbate into each well of the plate. The selection of 15 mol % was driven by empirical studies where <10 mol % peptide disallowed adhesion to spots containing growth factor peptides, and >50 mol % will facilitate nonspecific protein adsorption. The plate was gently rocked at room temperature for 1 h before spotting. An OmniGrid Microarrayer was then used to transfer nanoliter scale volumes of solution from the well plate onto the surface of the gold coverslips. After rinsing, the substrate was immersed overnight in a solution of HS-C11-EG3 to passivate the nonspotted regions and prevent nonspecific background adsorption. Since only nanoliters of solution are deposited during each print step, we were able to parafilm the master plates and store them at −20 °C. We found that the master plate could be reused months later with excellent reproducibility in terms of cell adhesion on the various peptides.

We stored the printed coverslips in 6-well plates and seeded B16F0 murine melanoma cells onto the substrates in normal serum-containing media at a concentration of 80 000 cells/mL. We found a concentration between 50 000 and 100 000 cells/mL was optimal for filling in all the spots without the cells becoming too confluent at the end of 5 days of culture. After seeding, the plate is gently shaken for a few minutes and then stored at 37 °C for 24 h. The next day we transferred the coverslips to a new 6-well plate. By doing so, we prevent cells that attach to the noncoverslip areas from growing confluent and expanding onto the printed array. After 5 days in culture, array coverslips were removed from media and fixed and stained for quantification. For every experiment, 3−6 replicates were printed; within each replicate array, columns represent repeat spots of each peptide combination (Figure 1b). Between replicates we see consistent differential adhesion of B16F0 melanoma cells to the peptide combinations, with some combinations promoting confluent spreading within each spot, and other peptides obstructing adhesion (Figure 1b insert).

Peptide Arrays for High Content Quantification of Cancer Cell Markers. To quantify immunofluorescence staining, the stained array coverslips were mounted with ProLong Diamond Antifade facedown onto glass slides and then imaged with a GE InCell 2000 high content imaging microscope at 10× magnification. A total of 144 images were taken of each substrate and stitched together in ImageJ to show the entire slide (Figure 1b). To quantify cells bound to each peptide, regions of interest were drawn around each spot.

DOI: 10.1021/acscentsci.6b00329
ACS Cent. Sci. 2017, 3, 381−393

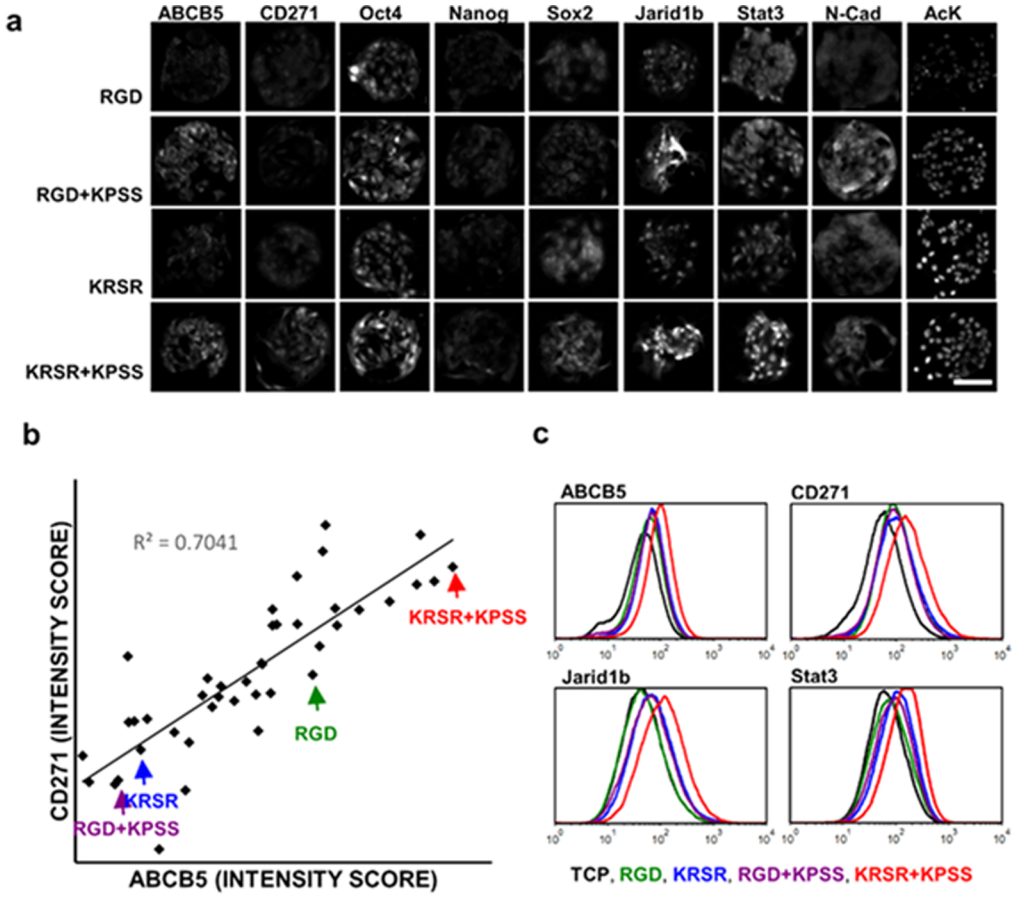

Figure 2. Representative images of a panel of putative melanoma cancer stem cell markers and markers associated with cancer stem cell phenotypes (a). A high correlation was found between CSC markers ABCB5 and CD271. Over three experimental repeats, the peptide combination KRSR + KPSS consistently showed high expression of both markers on the array (b). Nonpatterned peptide substrates for RGD, RGD + KPSS, KRSR, and KRSR + KPSS were used to culture large numbers of B16F0 cells for flow cytometry analysis (c). Flow cytometry confirms that cells cultured on KRSR + KPSS substrates display higher levels of ABCB5, CD271, Jarid1b, and Stat3. Scale bar = 100 μm.

Within each region of interest, the number of cells were counted by creating a mask of the DAPI channel. A profile of which peptide combinations support the most adhesion can be built by averaging the number of cells adhering to each spot. These adhesion profiles were highly reproducible between replicate slides as well as replicate experiments (Figure S1). Marker expression was quantified by measuring the integrated density (mean intensity × area) of the thresholded positive fluorescence (Figure S2). Each spot was then given an intensity score equal to the integrated density divided by the total area of the nuclei. These intensity scores were then averaged to give us a qualitative assessment of marker expression between various peptides. We found that, for spots with high confluency, stacking nuclei or nuclei in close proximity often resulted in undercounting of cells when we performed automatic segmentation. However, by measuring nuclear area and dividing by the average nuclear size, we were able to obtain nuclear counts for both high and low confluency spots that agreed well with manual nuclear counts (Figure S3). We also compared the marker expression intensity scores with the adhesion profile to see if higher marker expression was simply an artifact due to more cells being present. For eight of our nine markers examined, we saw little to no correlation (R^2 < 0.1) between marker expression intensity and adhesion (Figure S4). This analysis strategy facilitates high content analysis in a semi-quantitative high-throughput manner. After we have identified targets using immunofluorescence, we perform additional flow cytometry experiments using large surfaces conjugated with the peptides identified via screening, in order to attain more quantitative results on large numbers of cells.

As a model system to investigate how materials can influence cancer cell plasticity, we examined a variety of traditional stem cell markers such as OCT4, as well as putative MIC markers such as ABCB5 and CD271 (Figure 2a). ABCB5,[45] CD271,[46] and Jarid1b[47] are putative melanoma cancer stem cell markers. Oct4, Nanog, and Sox2 are general "stemness" markers, but aberrant expression has been associated with cancer stem cell phenotypes.[48,49] We focused on ABCB5 and CD271 and looked at the correlations between our panels of markers and these two well-documented MIC markers.[50] We observed a high correlation (R^2 = 0.70) between ABCB5 and CD271 (Figure 2b). We also see weak positive correlation between these two markers and Jarid1b, Stat3, and acetylated lysine (Figure S5). These are markers which we have previously shown can be upregulated via discrete biophysical parameters, and which promoted greater tumorigenicity in mice.[51] Our findings suggest that certain combinations of peptides promote upregulation of these MIC markers. A full list of the peptides with their marker expression intensity scores can be found in Supplemental Table 2 (Table S2).

From repeated experiments, we averaged the expression of these two markers (ABCB5, CD271) across all peptides. One

DOI: 10.1021/acscentsci.6b00329
ACS Cent. Sci. 2017, 3, 381−393

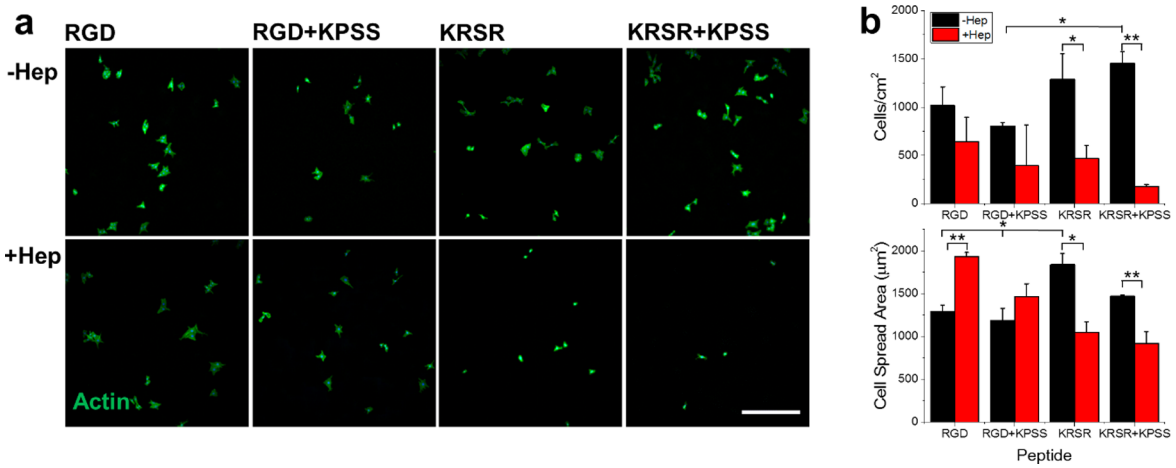

Figure 3. Actin staining of B16F0 cells on nonpatterned peptide SAMs with and without preincubation with soluble heparin (a). Quantification of cell density (cells/cm^2) and cell spread area (μm^2) on these surfaces (b). Scale bar = 500 μm. Error bars represent ± SEM *P < 0.05, **P < 0.01, based on one-way ANOVA with Tukey HSD post hoc testing.

unique peptide combination in particular, KRSR + KPSSAPTQLN (KRSR + KPSS), which consistently displays high levels of these MIC markers as well as general stem cell markers (Figure 2a,b, Table S1) was chosen to explore the role of these peptides in regulating the melanoma cell state. KRSR is a heparan sulfate binding peptide known to promote attachment of osteoblasts[37] while the KPSS peptide was first identified as a bioactive domain of bone morphogenetic protein-7 (BMP-7) and shown to promote osteoblastic adhesion and morphology.[41] The presence of this KPSS peptide in promoting CSC marker expression is interesting since BMP-7 has been shown to be implicated in melanoma tumor progression.[52] We cultured B16F0 cells on bulk SAM surfaces displaying the fibronectin derived adhesion sequence RGD, RGD + KPSS, KRSR, and KRSR + KPSS peptides and performed flow cytometry after 5 days. Similar to our immunofluorescent results from our peptide arrays, we observed similar elevated levels of putative MIC markers from cells cultured on KRSR + KPSS surfaces compared to those on control peptide surfaces. The KRSR + KPSS peptide combination displayed significantly higher expression levels of ABCB5, CD271, Jarid1b, and Stat3 compared to the RGD control peptide as well as just the KRSR peptide alone (Figure 2c). Interestingly, when we combine RGD with KPSS, we did not observe greater expression of these markers, suggesting that KRSR and KPSS uniquely exert synergistic interactions. To further verify the bioactivity of the KPSS sequence in promoting the MIC phenotype, we synthesized a scrambled version of the peptide, where amino-acids were exchanged N to C (KNPLSQSTAP (KPSS(Sc)). After 5 days of culture, cells adherent to KRSR+KPSS show elevated expression of MIC markers compared to cells cultured on both RGD + KPSS(Sc) and KRSR + KPSS(Sc) (Figure S6). This result supports a specific bioactivity associated with the KPSS sequence in mediating the MIC phenotype.

KRSR Mediates Melanoma Cell Adhesion through Proteoglycans. KRSR was first reported by Dee et al. as an adhesive peptide for osteoblast cells that promotes binding via a proteoglycan-mediated mechanism.[37] Subsequent studies using this peptide have mostly focused on osteoblasts, though we find that the KRSR peptide promotes adhesion of melanoma cells comparable to the RGD peptide (Figure 3a). We blocked the B16F0 cell membrane receptors by preincubating cells with soluble heparin at a concentration of 12 μg/mL and observed a 60% reduction in cell density after 24 h on gold substrates presenting the KRSR peptide, and a 85% reduction on substrates presenting the KRSR + KPSS peptides (Figure 3a,b). There were also marginal reductions in cell density on RGD and RGD + KPSS surfaces, though these changes were not significant (p > 0.05). After blocking with soluble heparin, the cells that remained attached to KRSR and KRSR + KPSS substrates were noticeably smaller and rounder in appearance and their average spread cell areas decreased from 1800 and 1500 μm^2 respectively, to 1000 and 900 μm^2 respectively. This trend was reversed on RGD and RGD + KPSS substrates, on which the average spread cell areas increased from 1300 and 1200 μm^2 respectively to 1900 and 1500 μm^2 respectively after preincubating with soluble heparin (Figure 3a,b). This result agrees with previous studies that cellular attachment to the fibronectin type III domain (FNIII, which contains the RGD motif) is mediated partially by cell surface proteoglycans. For example, Dalton et al. showed that the heparin-binding region of fibronectin interacts with cell-membrane proteoglycans to promote initial adhesion[53] while McCarthy et al. demonstrated that this same heparin-binding region alone could support adhesion and spreading of melanoma cells.[54] We should note that the KRSR peptide is highly charged, and we cannot rule out the influence of electrostatics in mediating other non-specific interactions with proteins in the media or on the cell surface. Nevertheless, we see a positive effect where heparin preincubation with melanoma cells seems to facilitate spreading to RGD-containing peptide substrates, whereas preincubation reduces binding to KRSR-containing substrates. This suggests that KRSR peptide and heparin directly compete for binding to cell-surface proteoglycans. In fact, if we preincubate the peptide substrate with soluble heparin, rather than the cells, we see slightly increased cell density on all peptide surfaces (Figure S7).

KPSSAPTQLN Promotes the Expression of Melanoma Stem Cell Markers. The KPSS peptide was first reported by Chen and Webster as a bioactive peptide derived from the knuckle epitope of BMP7 that could promote osteoblast adhesion, proliferation, alkaline phosphatase production, and calcium deposition.[41] We observed that this peptide, when immobilized onto a SAM by itself, failed to promote any adhesion of B16F0 cells (data not shown). However, using this

DOI: 10.1021/acscentsci.6b00329
ACS Cent. Sci. 2017, 3, 381−393

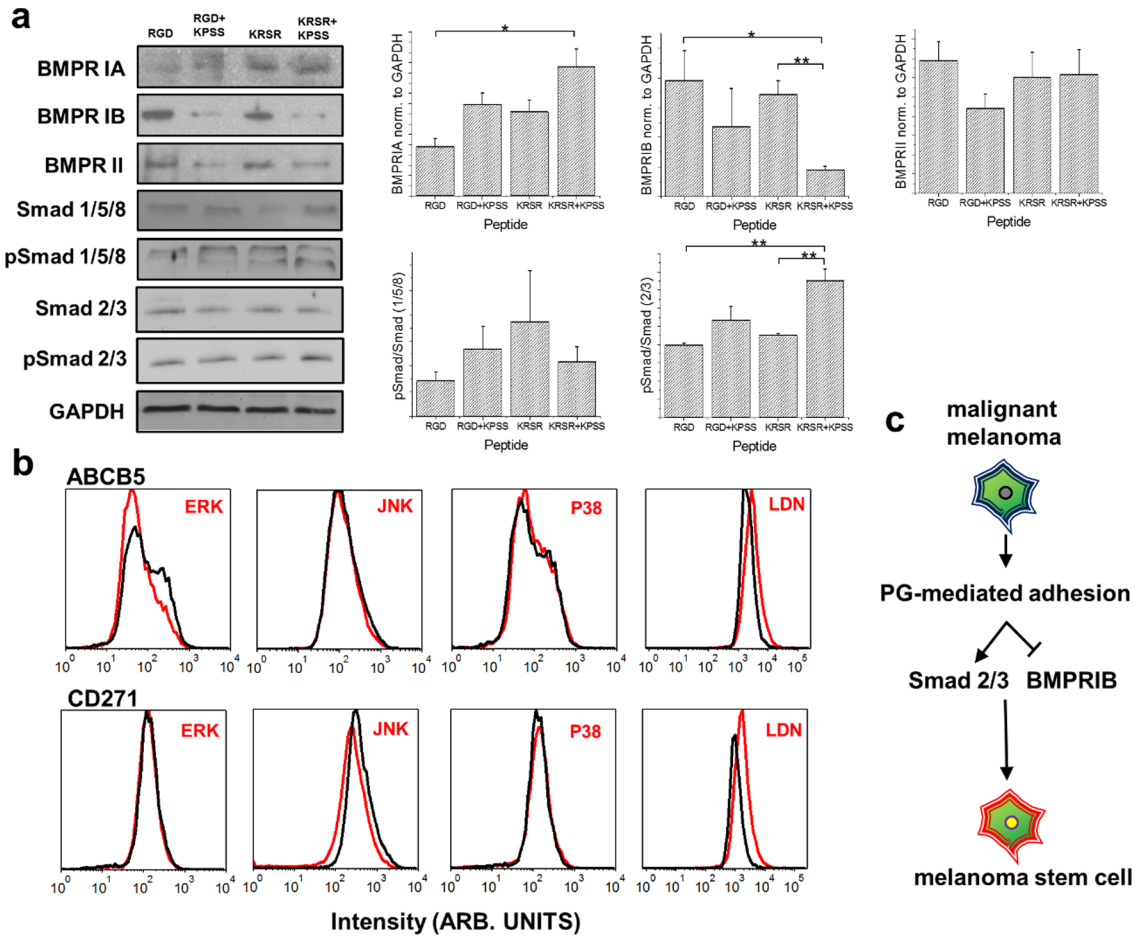

Figure 4. Western blots for BMP receptors and Smad proteins (a). BMPR quantification was normalized to GAPDH. Smad signaling was normalized by phosphorylated Smad against nonphosphorylated Smad. Flow cytometry histograms for B16F0 cells cultured for 5 days on nonpatterned peptide SAMs in the presence of pharmacological inhibitors for ERK, JNK, P38, and LDN-193189, an inhibitor of BMP type I receptors (b). Proposed pathway for peptide mediated signaling guiding CSC phenotype (c). Error bars represent ± SEM $*P < 0.05$, $**P < 0.01$, based on one-way ANOVA with Tukey HSD post hoc testing.

peptide combined with either RGD or KRSR does not impact cell adhesion or spreading (Figures 3a and S8a). We prepared SAM substrates bearing RGD and KRSR as single peptides and combined with the KPSS peptide, and cultured B16F0 cells on the substrates for 1, 3, or 5 days, after which we fixed and stained the substrates for ABCB5 and CD271. We observed that over the first 3 days of culture, all peptide conditions appear to have similar cell densities and low expression of ABCB5 and CD271. However, after 5 days in culture, the KRSR + KPSS peptide substrates induced significantly higher expression of both ABCB5 and CD271 (Figure S8b,c) that correlate well with immunofluorescence data from the peptide array (Figure 2a) as well as flow cytometry (Figure 2c). Since the KPSS peptide is derived from BMP7,[41] we investigated whether this peptide interacts with BMP receptors. We performed Western blot analysis of the three main BMP receptors: BMPRIA/ALK3, BMPRIB/ALK6, and BMPRII[55] for B16F0 melanoma cells cultured for 5 days on our peptide substrates. For cells grown on KRSR + KPSS substrates, we see slightly higher expression of BMPRIA and significantly lower expression of BMPRIB compared to RGD. There were no significant changes to expression of BMPRII across all peptides (Figure 4a). Interestingly, adding KPSS in conjunction with an adhesion promoting peptide increases BMPRIA expression and decreases BMPRIB expression. However, this trend was only significant for BMPRIB. We also attempted to visualize the interaction between the peptides and the receptors by adapting a method proposed by Schroeder et al. where cells and organelles are removed from the peptide substrate using a hypotonic solution, leaving only behind transmembrane proteins associated with the ventral side of the cell.[56] Rather than trypsinize the surface-bound receptors for mass spectrometry, we instead immunostained the proteins to quantify BMP receptors. We patterned discrete 5000 μm^2 peptide spots as previously described[57] to normalize total area and allow quantification of the BMP receptor intensities (Figure S9). Although we see high levels of background on control peptide surfaces, and a regional artifact at the perimeter of all samples, we observe a trend where the presence of KPSS peptide on the surface increases the appearance of associated BMPRIA, with a decrease in associated BMPRIB, similar to our western results (Figure 4a).

Downstream of BMP receptors, the canonical signaling pathway involves phosphorylation of Smads 1/5/8.[58] We performed Western blot analysis of phosphorylated and unphosphorylated Smads 1/5/8, and found no significant changes across the peptide surfaces when we compare the ratio of pSmad 1/5/8 to nonphospho Smad 1/5/8 (Figure 4a). We also performed Western blot analysis of phospho- and nonphospho- Smad 2/3 and observed increased Smad 2/3

DOI: 10.1021/acscentsci.6b00329
ACS Cent. Sci. 2017, 3, 381−393

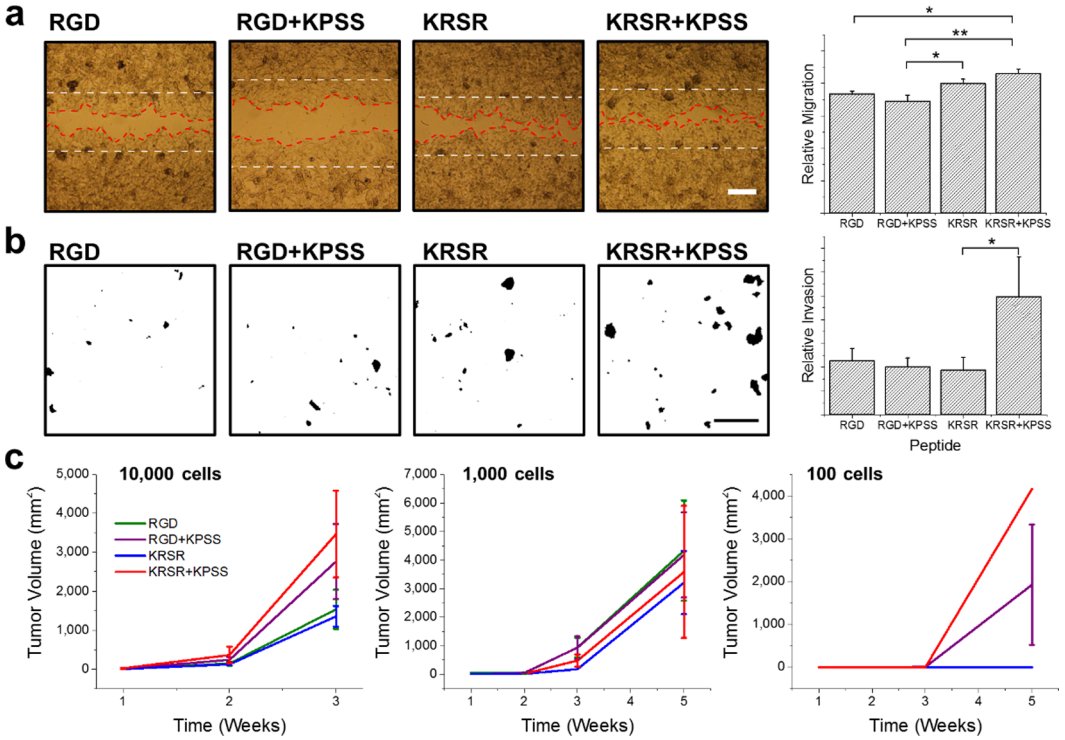

Figure 5. Wound healing and Boyden chamber invasion assay for B16F0 cells cultured on nonpatterned peptide substrates for 5 days. Wound healing scratches were imaged immediately and 12 h after initial scratch time to quantify relative migration (a). Relative invasion was quantified by measuring the total area of all cell nuclei that invade through the basement membrane 12 h after seeding (b). Average tumor volume (mm^2) in C57BL/6 mice that developed tumors after subcutaneous injection of B16F0 cells that had been cultured on nonpatterned peptide SAMs for 5 days (c). Scale bar = 200 μm. Error bars represent ± SEM *P < 0.05, **P < 0.01, based on one-way ANOVA with Tukey HSD post hoc testing.

signaling when the KPSS peptide is combined with a corresponding adhesion peptide (Figure 4a). This effect is most significant when KRSR is combined with KPSS (p < 0.01). Typically Smad 2/3 signaling is associated with TGFβ and activin receptor,[59] though BMPs have been shown to interact with TGFβ receptor type I to activate phosphorylation of Smad 2/3.[60] Cassar et al. showed that BMP7 could induce Smad3 phosphorylation in breast cancer cells, leading to cell senescence,[61] and Holtzhausen et al. recently reported that BMPs could induce Smad2/3 signaling, a process that preferentially occurs in cancer and embryonic cell lines. These collective findings suggest that during development BMPs typically signal through Smads 1/5/8, while in a more dedifferentiated phenotype, Smad 2/3 signaling is activated.[62] In our system, we observed the concurrent induction of Smad 2/3 signaling via a BMP7 derived peptide with an increase in the expression of MIC markers. At a peptide density of ∼15 mol % we would expect a relatively high number of peptides available for interaction with cell surface receptors, and the associated noncanonical Smad 2/3 signaling suggests receptor activation. However, we cannot discount the possibility of inhibitory interactions upon binding that may result in modulating Smad pathways, and the final phenotype observed.

Cell Binding to KPSSAPTQLN Peptide Influences Mitogen Activated Protein Kinase (MAPK) Activity. BMP receptors are a subset of the TGFβ superfamily of receptors and have been shown to have crosstalk with various other signaling pathways, particularly the MAP kinase pathways.[63] We used pharmacological inhibitors of ERK, JNK, and p38 MAP kinase and cultured B16F0 cells on peptide substrates for 5 days, before fixing and performing flow cytometry. With ERK inhibition, we see a decrease in ABCB5 expression but no change in CD271 of our melanoma cell population. With JNK inhibition we see a decrease in CD271 expression but no change in ABCB5 expression (Figure 4b). Unlike our previous report using patterned substrates which found the p38 MAP kinase pathway important in regulating the cancer stem cell phenotype,[51] no change in either ABCB5 or CD271 was observed following p38 inhibition. Interestingly, when we culture the B16F0 melanoma cells with LDN-193189, an inhibitor of BMP type I receptors,[64] we see an increase in ABCB5 and CD271 expression on both KRSR surfaces and on KRSR+KPSS surfaces (Figure 4b). This molecule targets BMPRIA and BMPRIB and inhibits phosphorylation of Smad 1/5/8.[64] However, we observe that inhibiting Smad 1/5/8 signaling increases the expression of CSC markers ABCB5 and CD271, suggesting canonical Smad 1/5/8 signaling may play a negative regulatory role in the MIC state, and further pointing to the role of Smad2/3 and MAP Kinase signaling in promoting the MIC phenotype for the KRSR+KPSS peptide combination (Figure 4c).

Culture on Peptide Substrates Influences Invasiveness in Vitro and in Vivo. To assess the invasiveness of melanoma cells cultured on the various peptide substrates in vitro, we performed wound healing and Boyden chamber invasion assays. For the wound healing assay, cells cultured on peptide SAMs for 5 days were trypsinized and reseeded at a concentration of 10^6 cells/mL onto glass coverslips to form a confluent monolayer. Three scratches were made onto each coverslip, and images of the initial scratch and scratch after 12 h were taken. We observed the highest relative migration from melanoma cells cultured on KRSR + KPSS peptide substrates

DOI: 10.1021/acscentsci.6b00329
ACS Cent. Sci. 2017, 3, 381−393

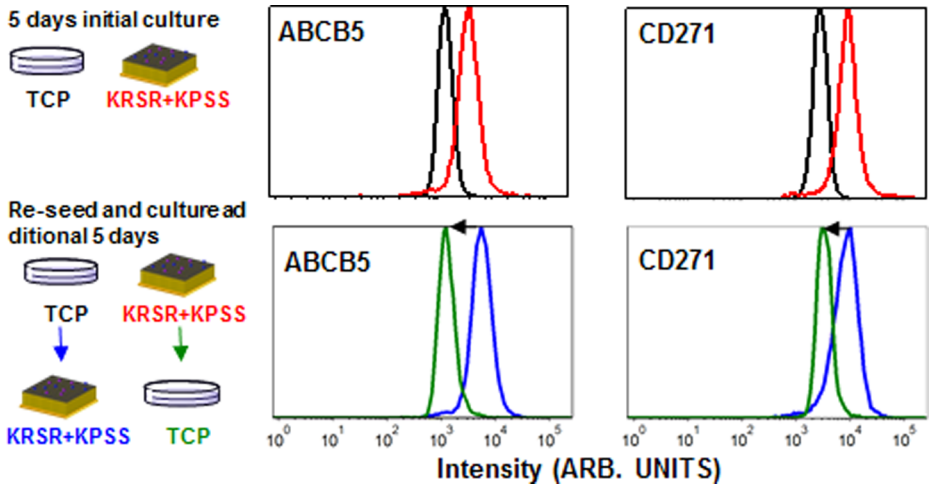

Figure 6. B16F0 cells were cultured for 5 days on either tissue culture plastic (TCP), or KRSR + KPSS nonpatterned SAM substrates. After 5 days of culture, cells were fixed for flow cytometry analysis, and 10 000 cells from each condition were reseeded onto either KRSR + KPSS (initially cultured on TCP), or onto TCP (initially cultured on KRSR + KPSS). After an additional 5 days of culture, these cells were fixed for flow cytometry analysis.

(Figure 5a). For the Boyden chamber invasion assay, we measured the ability of cells to invade through an artificial basement membrane. The migrated cells mostly formed colonies rather than remaining as single cells so we quantified invasion by the nuclear area of the invaded colonies. Similar to the scratch migration assay, the cells previously cultured on KRSR + KPSS substrates displayed the highest level of invasion (Figure 5b).

We performed in vivo tests for malignancy by culturing B16F0 cells on peptide SAM substrates for 5 days, followed by trypsinization and resuspension in HBSS buffer. Melanoma cells were injected into 6−8 week-old C57BL/6 mice subcutaneously and tumor growth was monitored twice per week with calipers. Mice injected with 10^4 cells quickly developed tumors and the mice in the experimental group were sacrificed after 3 weeks due to the large tumors in all mice groups at this time. After 3 weeks, the largest tumors occurred on mice injected with B16F0 cells previously cultured on KPSS-containing substrates, with the KRSR+KPSS condition group having the largest tumors (Figure 5c). However, when B16F0 inoculum was reduced to 10^3 and 10^2 cells, this trend was less evident with only a few mice developing tumors in the low injection number conditions (Figure S10a). We also assessed metastatic potency with a separate experiment in which we injected melanoma cells previously cultured on the four peptide combinations via tail vein injection into C57BL/6 mice. However, there was no difference in survival rate after 3 weeks between all the peptide conditions (Figure S10b). We tested cell viability to see if cells cultured on a particular peptide substrate were more prone to anoikis than others. We found no significant changes between the peptide surfaces, and >95% initial viability for all conditions. Even after suspension in HBSS buffer for 3 h (experimental injection condition), we see high cell viability for cells on all peptide surfaces (Figure S11).

Since preculture on peptide substrates does not show a pronounced difference in metastatic potency in vivo, we explored the plasticity of this state interconversion. We cultured B16F0 cells for 5 days on either tissue culture plastic (TCP) or KRSR + KPSS SAM substrates and observed higher ABCB5 and CD271 expression on cells cultured on KRSR+KPSS substrates (Figure 6). Cells from KRSR + KPSS were trypsinized and reseeded back onto TCP, while cells from TCP were trypsinized and reseeded onto new KRSR+KPSS substrates. The cells were allowed to culture for an additional 5 days, after which they were fixed and stained. For the cells that had previously been cultured on KRSR + KPSS and reseeded onto TCP, we see a complete shift in ABCB5 and CD271 to the levels of cells cultured initially for 5 days on TCP. Meanwhile, cells that had been cultured on TCP and then reseeded on KRSR + KPSS had the expected high expression of ABCB5 and CD271 (Figure 6). We cultured B16F0 cells on KRSR + KPSS substrates for 5 days and monitored ABCB5 and CD271 expression after removal for an additional 5 days. We see only small changes in expression levels after 1 day, but almost a complete reversal after 2 days (Figure S12). This reversal after 2 days likely explains why we see evidence of enhanced metastatic potency in the in vitro scratch and wound assays, and enhanced tumor growth in the subcutaneous in vivo assays, in which the cells are only removed from the KRSR +KPSS substrates for less than 24 h. For the syngeneic metastasis experiments, partial or full reversion of a MIC phenotype may occur after tail vein injection prior to extravasation into the lungs. Together, these results demonstrate that melanoma cells are highly plastic, and that their phenotype can be regulated through biochemical and biophysical cues. By investigating various peptide-presenting SAMs, we identify a unique combination which upregulates many putative cancer stem cell markers. Our results highlight the importance of heparin and proteoglycan-mediated adhesion, which when combined with a BMP7 derived morphogen motif, promotes noncannonical Smad 2/3 signaling to upregulate a malignant MIC phenotype (Figure 4c).

3. CONCLUSION

Signaling in the melanoma niche is viewed as a highly complex, and tightly coordinated process with multiple biophysical and biochemical cues presented in dynamic fashion. While combinatorial array approaches can be instructive in identifying peptide motifs that may be present during various stages of melanoma progression, there are clearly multiple signals in the melanoma niche that contribute to malignancy and tumorigenicity. We selected a panel of short peptides that are believed to be present within the melanoma microenvironment, and identified the BMP7 derived peptide KPSSAPTQLN as

DOI: 10.1021/acscentsci.6b00329
ACS Cent. Sci. 2017, 3, 381−393

mediating Smad 2/3 signaling and regulation of the MIC phenotype. Several previous reports have identified a role for BMP signaling in melanoma progression, including BMP7.[65,66] We propose that our peptide array approach can help select peptide motifs that may be involved in regulating distinct cellular states associated with progression, while providing designer surface coatings that can reproducibly augment a desired phenotype for therapeutic development. Furthermore, our results demonstrate the utility of a peptide microarray for normalizing a heterogeneous population of cancer cells and promoting a desired population.

The defined presentation and coaction of proteoglycan adhesion (KRSR) and stimulation of BMP receptors (KPSSAP-TQLN) activate Smad 2/3 signaling and MAPK activity to promote stem cell characteristics in populations of adherent melanoma cells. This finding suggests that BMP signaling in conjunction with proteoglycan adhesion within the tumor microenvironment may play a role in activating a stem-like MIC phenotype that is involved in progression. The enrichment of these MICs in vitro provides an opportunity to translate these tailored surfaces to develop therapeutics that target this population of cells believed to be at the heart of recurrence and metastasis. While we focused primarily on the KRSR+KPSS combination, we found numerous combinations that activate different markers associated with melanoma tumorigenicity and metastatic potential to various degrees. Therefore, we believe this microarray approach, that allows unambiguous exploration of discrete motifs, will find broad applicability in studies of precise ligand−receptor interactions that guide a cell state of interest. Furthermore, short peptides can be readily translated to a host of hydrogel chemistries toward the fabrication of three-dimensional materials that better recapitulate the biophysical and biochemical properties of the tumor microenvironment, toward the realization of synthetic in vitro avatars for therapeutic development on patient-derived cells.

4. EXPERIMENTAL SECTION

Materials. General laboratory chemicals and reagents were purchased from Sigma-Aldrich and Fisher Scientific unless otherwise specified. Peptide synthesis resin and amino acids were purchased from Anaspec. 11-(2-{2-[2-(2-Azido-ethoxy)-ethoxy]-ethoxy}-ethoxy)-undecane-1-thiol (referred to herein as HS-C11-EG4-N3) was purchased from Prochimia (Sopot, Poland, TH 008-m11.n4-0.2). Triethylene glycol mono-11-mercaptoundecyl ether (referred to herein as HS-C11-EG3) was purchased from Sigma-Aldrich (673110). Glass coverslips were purchased from Fisher Scientific. Cell culture plasticware was purchased from Denville Scientific. Cell culture media, fetal bovine serum (FBS), and penicillin/streptomycin (P/S) were purchased from Corning.

Cell Source and Culture. The B16F0 murine melanoma cell line was obtained from American Type Culture Collection. B16F0s were cultured in Dulbecco's Modified Eagle's Medium (DMEM) high glucose (4.5 g/mL) media supplemented with 10% FBS and P/S, media changed every 3 days, and passaged at ∼90% confluency every week using 0.05% trypsin. B16F0 cells were tested for mycoplasma contamination at Charles River Laboratories for cell line testing prior to in vivo experiments.

Peptide Synthesis. Peptides were synthesized manually by standard Fmoc solid-phase methodology as previously described.[25] Briefly, N-terminal fluorenylmethyloxycarbonyl (Fmoc) protected rink amide resin was deprotected with 20% piperidine in *N*′,*N*′-dimethylformamide (DMF) for 15 min. The solvent was filtered and the resin was washed 4 times with DMF. A solution containing 3 equiv of amino acid, benzotriazol-1-yl-oxytripyrrolidinophosphonium hexafluorophosphate (PyBOP), and *N*-methylmorpholine in DMF was then added and incubated at room temperature for 1 h with gentle rocking. After coupling, the resulting solution was filtered, the resin was washed 4 times with DMF, and the next Fmoc was deprotected. Coupling and deprotection was assessed using a ninhydrin test. After all amino acids were coupled, the peptides were capped with a propargyl-PEG-NHS ester (Quanta Biodesign, 10511) in DMF overnight. The resin was cleaved with a cocktail containing 95% trifluoroacetic acid (TFA), 2.5% H2O, and 2.5% triisopropylsilane (TIS) for 3 h and the peptides were filtered from the resin. The peptide was precipitated by adding ice-cold diethyl ether and after 3 dissolve/precipitate steps using TFA/ether, finally dissolved in water and lyophilized. Final products were analyzed with low resolution electrospray ionization (ESI) (Waters Quattro II) and semipreparative reversed-phase high-performance liquid chromatography (RP-HPLC) (PerkinElmer Flexar). All peptides used were purified to >90% purity as assessed by HPLC, dissolved in deionized H_2O, and stored at −20 °C. Bioactive peptides synthesized are listed in Table 1.

Gold Surface Preparation. Five nm of Cr followed by 20 nm of Au were deposited onto the surface of cleaned glass coverslips (60 × 24 × 0.1 mm dimensions). Gold coverslips were stored in a desiccator for up to 2 weeks before use. Prior to use, gold substrates were cleaned by briefly sonicating for 1 min in glacial acetic acid followed by 1 min in ethanol. Gold coverslips were cut to approximate size 24 × 24 mm using a diamond indenter and mounted onto 75 × 25 mm microscope slides by applying a thin layer of ethanol to the interface.

Peptide Microarray Formation. A panel of 12 peptides were used, in single and as a combination with the other 11 peptides, for a total of 78 peptide combinations. Peptide microarrays were printed as previously described.[25] Stock solutions of peptide ligand (1 mM in H_2O), Tris[(1-benzyl-1*H*-1,2,3-triazol-4-yl)methyl]amine (TBTA) (5 mM in DMSO/*t*-butyl alcohol (3:1)), and HS-C11-EG4-N3/HS-C11-EG3 (15% azide mole fraction in ethanol) solution were prepared. Click solution was prepared by combining TBTA solution with copper (10 mM CuBr, 10 mM sodium ascorbate in DMSO) solution (2:1 v/v). Peptide combinations (5 μL total), click solution (5 μL), and HS-C11-EG4-N3 solution (10 μL) were pipetted to a 384-well plate and incubated 1 h at room temperature with gentle rocking. A Gene Machines OGR-03 OmniGrid Microarrayer was used to print the solutions of the resulting plate in subarray format on the gold-coated surfaces. Each peptide combination was printed as a column of 6 replicate spots. The substrate was removed from the microscope slide and thoroughly rinsed with deionized H_2O followed by ethanol 4 times. After rinsing, printed substrates were immersed in a 0.1% ethylenediaminetetraacetic acid (EDTA) solution for 20 min, followed by another 4 rinse steps of H_2O/ethanol. Substrates were then immersed in a HS-C11-EG3 solution to render the nonprinted regions inert to nonspecific adsorption. In addition to the 78 peptide combinations, 3 negative controls (RDG, PBS, and HS-C11-EG4-N3) and 3 positive controls (GRGDS, YIGSR, IKVAV) were printed on each slide, giving 84 × 6 replicate spots = 504 total spots for each 25 × 25 mm coverslip. Printed peptide microarray substrates were transferred to 6-well plates and seeded with

DOI: 10.1021/acscentsci.6b00329
ACS Cent. Sci. 2017, 3, 381−393

B16F0 cells at a concentration of ∼80 000 cells/mL. After 24 h, microarray chips were transferred to new 6-well plates to prevent migration of cells attached to perimeter of the wells. Chips were cultured for an additional 4 days, with media change every 2 days.

Nonpatterned Self-Assembled Monolayers. For investigations of specific peptides outside the array, Au surfaces were immersed in 15% HS-C11-EG4-N3/HS-C11-EG3 overnight to form monolayers. Surfaces were rinsed with ethanol, dried with air, and cut to fit into 24-well or 6-well culture plates. Peptides were conjugated by incubating the monolayer surface to a 1:1 solution of click solution and peptide ligand solution for 12 h at room temperature.

Immunofluorescence. Cells were fixed with 4% paraformaldehyde for 20 min, followed by permeabilization with 0.1% Triton X-100 in PBS for 20 min, and blocked with 0.1% bovine serum albumin (BSA) in PBS for 30 min. Primary antibody labeling was performed in 0.1% BSA solution overnight at 4 °C. Secondary antibody labeling was performed similarly in 2% goat serum, 1% bovine serum albumin PBS solution for 1 h at room temperature. A full list of primary and secondary antibodies used is available in Supplemental Table 1 (Table S1). Samples were mounted using ProLong diamond antifade mountant (Thermo Fisher) and immunofluorescence microscopy was performed using an IN Cell Analyzer 2000 (GE) microscope. For peptide microarray surfaces, the entire area was imaged at 10× magnification and stitched together using ImageJ software. To quantify marker expression, a region of interest was drawn around each peptide spot (approximately 100 μm in diameter), and a threshold was set to determine positive signal. The total integrated density of signal (mean signal × area) of each spot was normalized to the number of cells in each spot to generate a signal intensity for each peptide spot. Since there was often poor segmentation of nuclei due to high confluency of cells in each spot, we used total nuclear area to normalize. For every antibody marker, a minimum of three array surfaces each containing six replicate spots was used.

Flow Cytometry. B16F0 cells cultured on 24 × 24 mm peptide-conjugated self-assembled monolayer substrates were detached with 0.05% trypsin and centrifuged. The resulting cell pellet was fixed in 4% paraformaldehyde for 20 min and permeabilized in 0.1% Triton X-100 in PBS for 20 min. Cells were blocked with 0.1% BSA in PBS for 30 min and stained with primary antibody in 0.1% BSA in PBS overnight at 4 °C. Secondary staining was performed in 2% goat serum, 1% BSA in PBS for 1 h at room temperature. Flow cytometry was performed with a BD LSR Fortessa Flow Cytometry Analyzer. Cells stained with secondary antibody but without primary antibodies were used as negative controls for gating.

Western Blotting. B16F0 cells cultured on 24 × 24 mm substrates were lysed with RIPA buffer containing protease inhibitors (Santa Cruz Biotechnology) according to manufacturer instructions. A BCA assay kit (Thermo Fisher) was used to normalize total protein between samples. Twenty μg whole cell lysate was resuspended in Laemmli buffer and boiled for 5 min before running on a PAGE 4−20% Tris-Glycine gel (Lonza) with Tris running buffer. The gel was blotted to a PVDF membrane using a semidry transfer system and blocked with 5% skim milk in TBST for 30 min. Membranes were exposed to primary antibody in 5% skim milk in TBST overnight on ice, washed 3 times with TBST, and incubated with goat antirabbit secondary antibody HRP conjugate (Thermo Fisher) for 1 h at room temperature. After washing the membranes three times with TBST, signal is visualized using SuperSignal West Pico Chemiluminescent substrate (Thermo Fisher).

Cell Deroofing Assay. PDMS stamps featuring circular patterns of 5000 μm^2 were used to generate peptide-terminated features as previously described.[57] Briefly, stamps were inked with an inking solution containing 15 mol % HS-C11-EG4-N3, 85 mol % HS-C11-EG3 in ethanol, dried under air, and applied to the surface of the gold. Surfaces were then rinsed and immersed overnight in HS-C11-EG3 solution to backfill nonpatterned regions. RGD, RGD + KPSS, KRSR, and KRSR + KPSS peptides were then conjugated to the patterned HS-C11-EG4-N3 regions via copper-catalyzed cycloaddition. Residual copper was removed with a 50 mM EDTA solution for 5 min. B16F0 cells were seeded onto the substrates and cultured for 5 days. Cells were ruptured and "deroofed" by treating for 5 min in sterile 20 mM NH_4OH followed by three rinses in DI H_2O followed by three rinses in PBS. The proteins left on the patterned substrate were fixed in 4% PFA for 10 min, blocked with 0.1% BSA for 20 min, and primary stained overnight with BMPR antibodies. Secondary staining was performed in 2% goat serum, 1% BSA in PBS for 1 h. Samples were mounted with Prolong Diamond antifade and imaged on the IN Cell Analyzer 2000.

Heparin Inhibition Assay. Heparin salt (Sigma H3149) was dissolved in deionized water, filtered through a 0.2 μm filter, and used at a final concentration of ∼12 μg/mL. B16F0 cells were precultured with heparin for 20 min at 37 °C before centrifuging and washing. Cells were then seeded onto peptide-conjugated SAMs at a density ∼1,000 cells/mL. After 24 h, surfaces were fixed with PFA, permeabilized, and stained with DAPI and Phalloidin.

Pharmacological Inhibition. MAP kinase inhibitors for ERK1/2 (FR180204), JNK (SP600125), and p38 (SB202190) were added to the media at 6 μM concentrations during initial seeding and every subsequent media change. LDN-193189 was used at a concentration of 30 nM. MG132 was preincubated with suspended B16F0 cells at a 1 μM concentration for 1 h, then removed prior to seeding. After 24 h, MG132 was added to the media at 0.5 μM concentration.

Wound Healing Assay. B16F0 cells were cultured on peptide SAM substrates for 5 days before trypsinization and replating onto glass substrates (10^6 cells per glass coverslip). On the coverslips cells were cultured for 12 h and allowed to grow to about 90% confluence. Three linear scratches were made to each coverslip using a pipet tip. Cells were allowed to migrate over a period of 12 h, and were observed under brightfield microscopy. Brightfield images of each scratch were taken at initial time and after 12 h. The total scratch area for each time point was determined by tracing the outline of the cells using ImageJ, and wound healing was quantitatively assessed by subtracting the final scratch area from the initial scratch area.

Boyden Chamber Invasion Assay. Invasion of B16F0 cells through matrigel was assessed using 24-well Boyden chambers (Corning) with 8 μm pore inserts. Chambers were precoated with a mixture of Cultrex Reduced Growth Factor Basement Membrane Extract (Trevigen) and cell media to form a final concentration of 4 mg/mL of basement membrane. Cells were cultured for 5 days on peptide SAM substrates and then trypsinized and reseeded in serum-free media into the upper chambers of each well. The lower chamber contained serum-containing media and provides the chemotactic gradient

DOI: 10.1021/acscentsci.6b00329
ACS Cent. Sci. 2017, 3, 381−393

to drive migration. Cells were cultured for 12 h before fixing with 4% paraformaldehyde. Cells on the upper surface of the membrane filter were removed and only cells that crossed the insets to the lower surface were stained with DAPI. Cells on the lower surface were imaged using the IN Cell 2000 and counted.

B16F0 Melanoma in Vivo Model. 6−8-week-old female C57BL/6 mice were purchased from Charles River Laboratories for in vivo studies. B16F0 cells were cultured on peptide SAM substrates for 5 days before trypsinization and resuspension in Hank's Balanced Salt Solution (HBSS) buffer. Primary localized tumors were established by subcutaneously injecting B16F0 cells (total cell numbers 10^5, 10^4, or 10^3) into the right lateral flank. Six mice were used for each condition. Macroscopic tumor growth was serially measured (maximal length and width) with calipers three times a week. Tumor growth was checked every 3 days and experiments were stopped when the first mouse of the respective series had a tumor exceeding 2,000 mm^3. Tumor volume was calculated using $V = (L \times W^2)/2$, where L is length and W is width. Criteria used for primary tumorigenesis was the formation of subcutaneous tumors which were detectable by visual examination and measurable with calipers. For comparison of primary tumor formation kinetics, mice were evaluated daily until primary tumors exceeded 20 mm in diameter, then humanely euthanized. Experimental metastases were established by injecting 10^5 B16F0 (grown on peptide SAM substrates) melanoma cells via lateral tail vein injection. The primary end point was survival time, and mice were monitored daily until reaching criteria for humane euthanasia. Inoculation of mice with melanoma cells grown on different conditions (peptide substrates) and different cell densities was not performed in a random fashion. Rather, cohorts of mice were predetermined to receive injections of melanoma cells grown under specified conditions and cell densities before inoculation. All experiments using live animals were in compliance with animal welfare ethical regulations and approved by the Institute Animal Care and Use Committee before experimentation.

Statistical Analysis. Data from three independent experiments were compared and expressed as mean ± standard error of the mean (s.e.m.) unless otherwise specified. Statistical tests were performed in OriginPro using Student's t test for comparisons between two groups, and one-way analysis of variance (ANOVA) with Tukey HSD Posthoc analysis for multiple comparisons.

■ ASSOCIATED CONTENT

Supporting Information

The Supporting Information is available free of charge on the ACS Publications website at DOI: 10.1021/acscentsci.6b00329.

Additional figures and tables (PDF)

■ AUTHOR INFORMATION

Corresponding Author

*E-mail: kakilian@illinois.edu.

ORCID

Kristopher A. Kilian: 0000-0002-8963-9796

Author Contributions

D.Z. and K.A.K. conceived the ideas and designed the experiments. D.Z., J.L., M.B.S., Y.P., J.C., and T.M.F. conducted the experiments. D.Z., J.L, T.M.F., and K.A.K. analyzed the data. All authors contributed to interpreting data and writing the manuscript.

Funding

This work was supported by the National Science Foundation grant number 1454616.

Notes

The authors declare no competing financial interest.

■ REFERENCES

(1) Schadendorf, D.; Fisher, D. E.; Garbe, C.; Gershenwald, J. E.; Grob, J.-J.; Halpern, A.; Herlyn, M.; Marchetti, M. A.; McArthur, G.; Ribas, A.; et al. Melanoma. *Nat. Rev. Dis. Prim.* **2015**, *1*, 15003.

(2) Schatton, T.; Murphy, G. F.; Frank, N. Y.; Yamaura, K.; Waaga-Gasser, A. M.; Gasser, M.; Zhan, Q.; Jordan, S.; Duncan, L. M.; Weishaupt, C.; et al. Identification of cells initiating human melanomas. *Nature* **2008**, *451*, 345−349.

(3) Reya, T.; Morrison, S. J.; Clarke, M. F.; Weissman, I. L. Stem cells, cancer, and cancer stem cells. *Nature* **2001**, *414*, 105−111.

(4) Clevers, H. The cancer stem cell: premises, promises and challenges. *Nat. Med.* **2011**, *17*, 313−319.

(5) Quintana, E.; Shackleton, M.; Sabel, M. S.; Fullen, D. R.; Johnson, T. M.; Morrison, S. J. Efficient tumour formation by single human melanoma cells. *Nature* **2008**, *456*, 593−598.

(6) Quintana, E.; Shackleton, M.; Foster, H. R.; Fullen, D. R.; Sabel, M. S.; Johnson, T. M.; Morrison, S. J. Phenotypic heterogeneity among tumorigenic melanoma cells from patients that is reversible and not hierarchically organized. *Cancer Cell* **2010**, *18*, 510−523.

(7) Dirks, P. Cancer stem cells: Invitation to a second round. *Nature* **2010**, *466*, 40−41.

(8) Girouard, S. D.; Murphy, G. F. Melanoma stem cells: not rare, but well done. *Lab. Invest.* **2011**, *91*, 647−664.

(9) Gupta, P. B.; Chaffer, C. L.; Weinberg, R. A. Cancer stem cells: mirage or reality? *Nat. Med.* **2009**, *15*, 1010−1012.

(10) Allen, M.; Jones, J. L. Jekyll and Hyde: the role of the microenvironment on the progression of cancer. *J. Pathol.* **2011**, *223*, 163−177.

(11) Klein-Goldberg, A.; Maman, S.; Witz, I. P. The role played by the microenvironment in site-specific metastasis. *Cancer Lett.* **2014**, *352*, 54−58.

(12) Korkaya, H.; Liu, S.; Wicha, M. S. Breast cancer stem cells, cytokine networks, and the tumor microenvironment. *J. Clin. Invest.* **2011**, *121*, 3804−3809.

(13) Desgrosellier, J. S.; Cheresh, D. A. Integrins in cancer: biological implications and therapeutic opportunities. *Nat. Rev. Cancer* **2010**, *10*, 9−22.

(14) Bergamaschi, A.; Tagliabue, E.; Sørlie, T.; Naume, B.; Triulzi, T.; Orlandi, R.; Russnes, H.; Nesland, J.; Tammi, R.; Auvinen, P.; et al. Extracellular matrix signature identifies breast cancer subgroups with different clinical outcome. *J. Pathol.* **2008**, *214*, 357−367.

(15) Vera-Ramirez, L.; Sanchez-Rovira, P.; Ramirez-Tortosa, C. L.; Quiles, J. L.; Ramirez-Tortosa, M. C.; Alvarez, J. C.; Fernandez-Navarro, M.; Lorente, J. A. Gene-expression profiles, tumor microenvironment, and cancer stem cells in breast cancer: latest advances towards an integrated approach. *Cancer Treat. Rev.* **2010**, *36*, 477−484.

(16) Anderson, D. G.; Levenberg, S.; Langer, R. Nanoliter-scale synthesis of arrayed biomaterials and application to human embryonic stem cells. *Nat. Biotechnol.* **2004**, *22*, 863−866.

(17) Gobaa, S.; Hoehnel, S.; Roccio, M.; Negro, A.; Kobel, S.; Lutolf, M. P. Artificial niche microarrays for probing single stem cell fate in high throughput. *Nat. Methods* **2011**, *8*, 949−955.

(18) Orner, B. P.; Derda, R.; Lewis, R. L.; Thomson, J. A.; Kiessling, L. L. Arrays for the combinatorial exploration of cell adhesion. *J. Am. Chem. Soc.* **2004**, *126*, 10808−10809.

(19) Derda, R.; Musah, S.; Orner, B. P.; Klim, J. R.; Li, L.; Kiessling, L. L. High-throughput discovery of synthetic surfaces that support proliferation of pluripotent cells. *J. Am. Chem. Soc.* **2010**, *132*, 1289−1295.

(20) Carragher, N. O. Profiling distinct mechanisms of tumour invasion for drug discovery: imaging adhesion, signalling and matrix turnover. *Clin. Exp. Metastasis* **2009**, *26*, 381−397.

DOI: 10.1021/acscentsci.6b00329
ACS Cent. Sci. 2017, 3, 381−393

(21) Reticker-Flynn, N. E.; Malta, D. F. B.; Winslow, M. M.; Lamar, J. M.; Xu, M. J.; Underhill, G. H.; Hynes, R. O.; Jacks, T. E.; Bhatia, S. N. A combinatorial extracellular matrix platform identifies cell-extracellular matrix interactions that correlate with metastasis. *Nat. Commun.* **2012**, *3*, 1122.
(22) Barney, L. E.; Dandley, E. C.; Jansen, L. E.; Reich, N. G.; Mercurio, A. M.; Peyton, S. R. A cell-ECM screening method to predict breast cancer metastasis. *Integr. Biol. (Camb)* **2015**, *7*, 198−212.
(23) Postovit, L.-M.; Seftor, E. a; Seftor, R. E. B.; Hendrix, M. J. C. A three-dimensional model to study the epigenetic effects induced by the microenvironment of human embryonic stem cells. *Stem Cells* **2006**, *24*, 501−505.
(24) Postovit, L.-M.; Seftor, E. A.; Seftor, R. E. B.; Hendrix, M. J. C. Influence of the microenvironment on melanoma cell fate determination and phenotype. *Cancer Res.* **2006**, *66*, 7833−7836.
(25) Zhang, D.; Kilian, K. A. Peptide microarrays for the discovery of bioactive surfaces that guide cellular processes: a single step azide−alkyne "click" chemistry approach. *J. Mater. Chem. B* **2014**, *2*, 4280.
(26) Kilian, K. A.; Mrksich, M. Directing stem cell fate by controlling the affinity and density of ligand-receptor interactions at the biomaterials interface. *Angew. Chem., Int. Ed.* **2012**, *51*, 4891−4895.
(27) Bilem, I.; Chevallier, P.; Plawinski, L.; Sone, E. D.; Durrieu, M. C.; Laroche, G. RGD and BMP-2 mimetic peptide crosstalk enhances osteogenic commitment of human bone marrow stem cells. *Acta Biomater.* **2016**, *36*, 132−142.
(28) Lee, J. S.; Lee, J. S.; Wagoner-Johnson, A.; Murphy, W. L. Modular peptide growth factors for substrate-mediated stem cell differentiation. *Angew. Chem., Int. Ed.* **2009**, *48*, 6266−6269.
(29) Koepsel, J. T.; Nguyen, E. H.; Murphy, W. L. Differential effects of a soluble or immobilized VEGFR-binding peptide. *Integr. Biol.* **2012**, *4*, 914.
(30) He, X.; Ma, J.; Jabbari, E. Effect of grafting RGD and BMP-2 protein-derived peptides to a hydrogel substrate on osteogenic differentiation of marrow stromal cells. *Langmuir* **2008**, *24*, 12508−12516.
(31) Kim, S.-H.; Turnbull, J.; Guimond, S. Extracellular matrix and cell signalling: the dynamic cooperation of integrin, proteoglycan and growth factor receptor. *J. Endocrinol.* **2011**, *209*, 139−151.
(32) Pinho, S. S.; Reis, C. A. Glycosylation in cancer: mechanisms and clinical implications. *Nat. Rev. Cancer* **2015**, *15*, 540−555.
(33) Pierschbacher, M. D.; Ruoslahti, E. Cell attachment activity of fibronectin can be duplicated by small synthetic fragments of the molecule. *Nature* **1984**, *309*, 30−33.
(34) Graf, J.; Iwamoto, Y.; Sasaki, M.; Martin, G. R.; Kleinman, H. K.; Robey, F. A.; Yamada, Y. Identification of an amino acid sequence in laminin mediating cell attachment, chemotaxis, and receptor binding. *Cell* **1987**, *48*, 989−996.
(35) Tashiro, K.; Sephel, G.; Weeks, B.; Sasaki, M.; Martin, G.; Kleinman, H.; Yamada, Y. A synthetic peptide containing the IKVAV sequence from the A chain of laminin mediates cell attachment, migration, and neurite outgrowth. *J. Biol. Chem.* **1989**, *264*, 16174−16182.
(36) Underwood, P. A.; Bennett, F. A.; Kirkpatrick, A.; Bean, P. A.; Moss, B. A. Evidence for the location of a binding sequence for the alpha 2 beta 1 integrin of endothelial cells, in the beta 1 subunit of laminin. *Biochem. J.* **1995**, *309*, 765−771.
(37) Dee, K. C.; Andersen, T. T.; Bizios, R. Design and function of novel osteoblast-adhesive peptides for chemical modification of biomaterials. *J. Biomed. Mater. Res.* **1998**, *40*, 371−377.
(38) Rezania, A.; Healy, K. E. Biomimetic peptide surfaces that regulate adhesion, spreading, cytoskeletal organization, and mineralization of the matrix deposited by osteoblast-like cells. *Biotechnol. Prog.* **1999**, *15*, 19−32.
(39) Guo, N. H.; Krutzsch, H. C.; Nègre, E.; Vogel, T.; Blake, D. A.; Roberts, D. D. Heparin- and sulfatide-binding peptides from the type I repeats of human thrombospondin promote melanoma cell adhesion. *Proc. Natl. Acad. Sci. U. S. A.* **1992**, *89*, 3040−3044.
(40) Lee, J.-Y.; Choo, J.-E.; Choi, Y.-S.; Suh, J.-S.; Lee, S.-J.; Chung, C.-P.; Park, Y.-J. Osteoblastic differentiation of human bone marrow stromal cells in self-assembled BMP-2 receptor-binding peptide-amphiphiles. *Biomaterials* **2009**, *30*, 3532−3541.
(41) Chen, Y.; Webster, T. J. Increased osteoblast functions in the presence of BMP-7 short peptides for nanostructured biomaterial applications. *J. Biomed. Mater. Res., Part A* **2009**, *91*, 296−304.
(42) Yamada, K. M.; Miyamoto, S. Integrin transmembrane signaling and cytoskeletal control. *Curr. Opin. Cell Biol.* **1995**, *7*, 681−689.
(43) Alam, N.; Goel, H. L.; Zarif, M. J.; Butterfield, J. E.; Perkins, H. M.; Sansoucy, B. G.; Sawyer, T. K.; Languino, L. R. The integrin-growth factor receptor duet. *J. Cell. Physiol.* **2007**, *213*, 649−653.
(44) Rosso, F.; Giordano, A.; Barbarisi, M.; Barbarisi, A. From cell-ECM interactions to tissue engineering. *J. Cell. Physiol.* **2004**, *199*, 174−180.
(45) Frank, N. Y.; Margaryan, A.; Huang, Y.; Schatton, T.; Waaga-Gasser, A. M.; Gasser, M.; Sayegh, M. H.; Sadee, W.; Frank, M. H. ABCB5-mediated doxorubicin transport and chemoresistance in human malignant melanoma. *Cancer Res.* **2005**, *65*, 4320−4333.
(46) Boiko, A. D.; Razorenova, O. V.; van de Rijn, M.; Swetter, S. M.; Johnson, D. L.; Ly, D. P.; Butler, P. D.; Yang, G. P.; Joshua, B.; Kaplan, M. J.; et al. Human melanoma-initiating cells express neural crest nerve growth factor receptor CD271. *Nature* **2010**, *466*, 133−137.
(47) Roesch, A.; Fukunaga-Kalabis, M.; Schmidt, E. C.; Zabierowski, S. E.; Brafford, P. a; Vultur, A.; Basu, D.; Gimotty, P.; Vogt, T.; Herlyn, M. A temporarily distinct subpopulation of slow-cycling melanoma cells is required for continuous tumor growth. *Cell* **2010**, *141*, 583−594.
(48) Ben-Porath, I.; Thomson, M. W.; Carey, V. J.; Ge, R.; Bell, G. W.; Regev, A.; Weinberg, R. A. An embryonic stem cell-like gene expression signature in poorly differentiated aggressive human tumors. *Nat. Genet.* **2008**, *40*, 499−507.
(49) Kumar, S. M.; Liu, S.; Lu, H.; Zhang, H.; Zhang, P. J.; Gimotty, P. A.; Guerra, M.; Guo, W.; Xu, X. Acquired cancer stem cell phenotypes through Oct4-mediated dedifferentiation. *Oncogene* **2012**, *31*, 4898−4911.
(50) Medema, J. P. Cancer stem cells: the challenges ahead. *Nat. Cell Biol.* **2013**, *15*, 338−344.
(51) Lee, J.; Abdeen, A. A.; Wycislo, K. L.; Fan, T. M.; Kilian, K. A. Interfacial geometry dictates cancer cell tumorigenicity. *Nat. Mater.* **2016**, *15*, 856−862.
(52) Hsu, M.-Y.; Rovinsky, S. A.; Lai, C.-Y.; Qasem, S.; Liu, X.; How, J.; Engelhardt, J. F.; Murphy, G. F. Aggressive melanoma cells escape from BMP7-mediated autocrine growth inhibition through coordinated Noggin upregulation. *Lab. Invest.* **2008**, *88*, 842−855.
(53) Dalton, B. A.; McFarland, C. D.; Underwood, P. A.; Steele, J. G. Role of the heparin binding domain of fibronectin in attachment and spreading of human bone-derived cells. *J. Cell Sci.* **1995**, *108*, 2083−2092.
(54) McCarthy, J. B.; Hagen, S. T.; Furcht, L. T. Human fibronectin contains distinct adhesion- and motility-promoting domains for metastatic melanoma cells. *J. Cell Biol.* **1986**, *102*, 179−188.
(55) Rahman, M. S.; Akhtar, N.; Jamil, H. M.; Banik, R. S.; Asaduzzaman, S. M. TGF-β/BMP signaling and other molecular events: regulation of osteoblastogenesis and bone formation. *Bone Res.* **2015**, *3*, 15005.
(56) Todorović, V.; Desai, B. V.; Eigenheer, R. A.; Yin, T.; Amargo, E. V.; Mrksich, M.; Green, K. J.; Patterson, M. J. S. Detection of differentially expressed basal cell proteins by mass spectrometry. *Mol. Cell. Proteomics* **2010**, *9*, 351−361.
(57) Zhang, D.; Sun, M. B.; Lee, J.; Abdeen, A. A.; Kilian, K. A. Cell shape and the presentation of adhesion ligands guide smooth muscle myogenesis. *J. Biomed. Mater. Res., Part A* **2016**, *104*, 1212−1220.
(58) Massagué, J. TGF-beta signal transduction. *Annu. Rev. Biochem.* **1998**, *67*, 753−791.
(59) Nohe, A.; Hassel, S.; Ehrlich, M.; Neubauer, F.; Sebald, W.; Henis, Y. I.; Knaus, P. The mode of bone morphogenetic protein (BMP) receptor oligomerization determines different BMP-2 signaling pathways. *J. Biol. Chem.* **2002**, *277*, 5330−5338.

DOI: 10.1021/acscentsci.6b00329
ACS Cent. Sci. 2017, 3, 381−393

(60) Sieber, C.; Kopf, J.; Hiepen, C.; Knaus, P. Recent advances in BMP receptor signaling. *Cytokine Growth Factor Rev.* **2009**, *20*, 343−355.
(61) Cassar, L.; Nicholls, C.; Pinto, A. R.; Li, H.; Liu, J.-P. Bone morphogenetic protein-7 induces telomerase inhibition, telomere shortening, breast cancer cell senescence, and death via Smad3. *FASEB J. Off. Publ. Fed. Am. Soc. Exp. Biol.* **2009**, *23*, 1880−1892.
(62) Holtzhausen, A.; Golzio, C.; How, T.; Lee, Y.-H.; Schiemann, W. P.; Katsanis, N.; Blobe, G. C. Novel bone morphogenetic protein signaling through Smad2 and Smad3 to regulate cancer progression and development. *FASEB J.* **2014**, *28*, 1248−1267.
(63) Zhang, Y. E. Non-Smad pathways in TGF-beta signaling. *Cell Res.* **2009**, *19*, 128−139.
(64) Cuny, G. D.; Yu, P. B.; Laha, J. K.; Xing, X.; Liu, J.-F.; Lai, C. S.; Deng, D. Y.; Sachidanandan, C.; Bloch, K. D.; Peterson, R. T. Structure−activity relationship study of bone morphogenetic protein (BMP) signaling inhibitors. *Bioorg. Med. Chem. Lett.* **2008**, *18*, 4388−4392.
(65) Hsu, M. Y.; Rovinsky, S.; Penmatcha, S.; Herlyn, M.; Muirhead, D. Bone morphogenetic proteins in melanoma: Angel or devil? *Cancer Metastasis Rev.* **2005**, *24*, 251−263.
(66) Rothhammer, T.; Poser, I.; Soncin, F.; Bataille, F.; Moser, M.; Bosserhoff, A.-K. Bone Morphogenic Proteins Are Overexpressed in Malignant Melanoma and Promote Cell Invasion and Migration. *Cancer Res.* **2005**, *65*, 448−456.

DOI: 10.1021/acscentsci.6b00329
ACS Cent. Sci. 2017, 3, 381−393